Supplement of Atmos. Chem. Phys., 22, 2525–2552, 2022
https://doi.org/10.5194/acp-22-2525-2022-supplement

Atmospheric Chemistry and Physics
Open Access
EGU

Supplement of

Plant gross primary production, plant respiration and carbonyl sulfide emissions over the globe inferred by atmospheric inverse modelling

Marine Remaud et al.

Correspondence to: Marine Remaud (mremaud@lsce.ipsl.fr)

Supplement

Marine Remaud

Correspondence: marine.remaud@lsce.ipsl.fr

A GPP estimates

GPP Estimate (PgC/yr) +/-SD	Method	Duration (Years)	Citation
110 +/- 11	MODIS	1982-2012	Zhao et al.
128 +/- 4	Neural Network	1998-2005	Beer et al.
124 +/- 7	Water Use Efficiency	1998-2005	Beer et al.
106 +/- 6	Light Use Efficiency	1998-2005	Beer et al.
119 +/- 6	Upscaled Flux Tower	1982-2008	Jung et al.
129 +/- 16	Oxygen isotopes in H_2O	1968-2013	Jasechko et al.
162.5 +/- 6	Oxygen isotopes in CO_2	1990-2010	Welp et al.
122 +/- 2.4	Solar Induced Fluorescence (WECAN)	2010-2015	Alemohammad
125 +/- 12	Process BESS Model	1982-2015	Ryu et al.
147 +/- 8	Near Infrared (NIRv)		Badgley et al.
125 +/- 5.2	***MODIS- soil moisture constrained***	1982-2016	Stocker et al.
130 +/- 17	***Inverse Variance Weighted Estimate***		

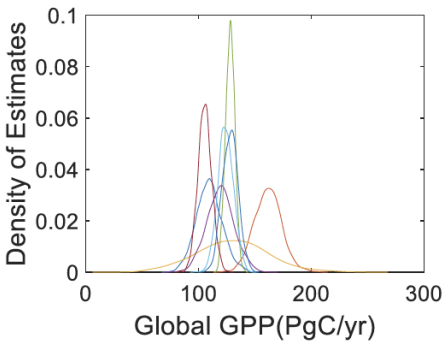

Figure S1. Left: compilation of GGP estimates from recent litterature. Right: Distribution of these GPP estimates, assuming they are gaussian with a standard deviation equal to the uncertainties on the tabular. From Ashley Ballentyne personnal presentation

B Observation footprints

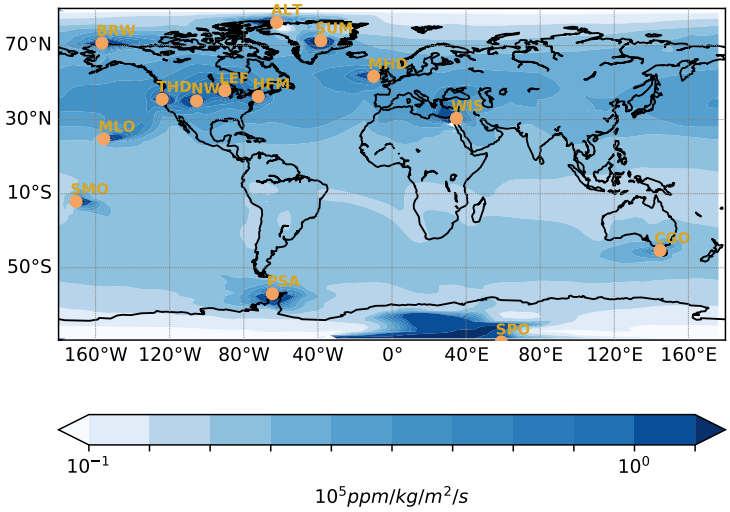

Figure S2. Annual climatology of Jacobians computed by the adjoint of the LMDz model: map of the partial derivatives, in $\mathrm{ppm}/(\mathrm{kg}/\mathrm{m}^2/\mathrm{s})$, of a monthly mean concentration at all stations from the NOAA network with respect to CO_2 surface fluxes in the nine previous months. The yellow dots denote the location of the surface sites. The site KUM is not depicted as it has the same coordinates than MLO.

C Evaluation of the reconstructed adjoint transport

We check here that the reconstructed transport using the adjoint transport is consistent with the full LMdz transport. Figure S3 shows a comparison of the CO_2 concentrations given by the adjoint of LMDz against concentrations simulated by the forward LMDz ATM at surface. The adjoint transport and the forward model are in almost total agreement at all stations.

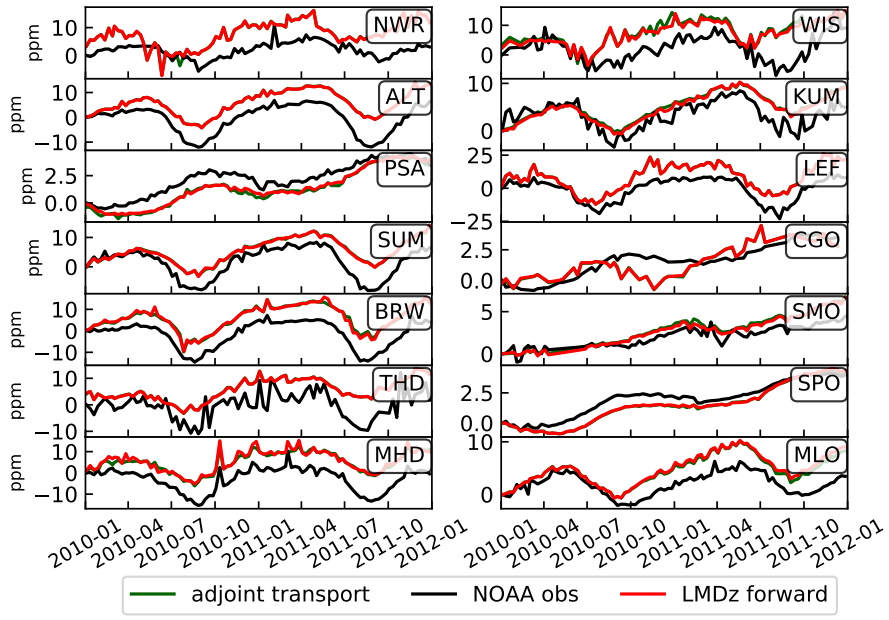

Figure S3. Temporal series of observed (black) and simulated CO_2 (green and red) concentrations at surface sites from the NOAA network. The red curve corresponds to the concentrations simulated by the full atmospheric transport. The green curve corresponds to the concentrations given by backward integration of the adjoint transport combined to the prior fluxes (reconstructed transport).

D Prior and posterior CO_2 and COS budgets

E Supplementary figures of the section 3.3.2 : Evaluation of the simulated vertical profiles against NOAA/ESRL airborne measurements

The used observation programme here is the NOAA Earth System Research Laboratory (ESRL) Global Greenhouse Gas Reference Network Aircraft Program. It provides information about the vertical profiles of CO_2 and COS (Montzka et al., 2007; Campbell et al., 2008; Ma et al., 2020). It consists here of measurements of air samples collected by flasks every few days or months at 16 aircraft profiling sites over continental and coastal North America between 2008 and 2011 between altitudes of 300 and 8000 m above sea level.

CO2 GPP [GtC/y]

PFT	Prior	Post
10 TeC3g	-4.9	-3.7
11 C4g	-19.0	-19.0
12 C3Ag	-15.3	-15.3
13 C4Ag	-7.1	-7.0
14 TrC3g	-1.7	-1.6
15 BoC3g	-4.5	-4.3
2 TrBrE	-35.7	-33.3
3 TrBrR	-10.4	-9.2
4 TeNeE	-4.0	-3.0
5 TeBrE	-6.1	-4.8
6 TeBrS	-5.5	-4.9
7 BoNeE	-5.8	-7.2
8 BoBrS	-3.8	-4.3
9 BoNeS	-1.3	-1.5

CO2 Respiration [GtC/y]

PFT	Prior	Post
1 BaSoil	0.2	0.2
10 TeC3g	5.4	4.6
11 C4g	19.6	17.0
12 C3Ag	13.4	9.8
13 C4Ag	5.8	5.3
14 TrC3g	2.1	2.0
15 BoC3g	4.7	5.3
2 TrBrE	35.8	35.1
3 TrBrR	10.4	9.9
4 TeNeE	4.0	4.1
5 TeBrE	6.1	5.4
6 TeBrS	5.4	4.7
7 BoNeE	5.5	5.3
8 BoBrS	3.6	3.7
9 BoNeS	1.2	1.1

Vegetation sink [GgS/y]

PFT	Prior	Post
10 TeC3g	-27.4	-20.6
11 C4g	-77.3	-77.1
12 C3Ag	-85.6	-84.8
13 C4Ag	-28.4	-27.9
14 TrC3g	-9.7	-8.7
15 BoC3g	-24.9	-23.8
2 TrBrE	-201.6	-187.9
3 TrBrR	-59.1	-51.8
4 TeNeE	-22.0	-16.6
5 TeBrE	-34.2	-26.8
6 TeBrS	-30.7	-27.3
7 BoNeE	-32.3	-39.9
8 BoBrS	-21.1	-23.7
9 BoNeS	-7.1	-8.4

COS Soil fluxes [GgS/y]

PFT	Prior	Post
10 TeC3g	-21.0	-15.1
11 C4g	-25.9	-24.6
12 C3Ag	-11.3	-11.0
13 C4Ag	-1.5	-1.5
14 TrC3g	-17.7	-15.7
15 BoC3g	-33.3	-31.2
2 TrBrE	-24.0	-21.3
3 TrBrR	-21.3	-18.9
4 TeNeE	-12.3	-9.7
5 TeBrE	-12.0	-9.1
6 TeBrS	-14.6	-11.7
7 BoNeE	-18.0	-17.1
8 BoBrS	-14.4	-14.0
9 BoNeS	-9.7	-9.5

Figure S4. Top: Distribution of the average total yearly GPP and respiration per PFT in GtC Bottom: Distribution of the average total yearly vegetation and soil COS fluxes per PFT in GgS

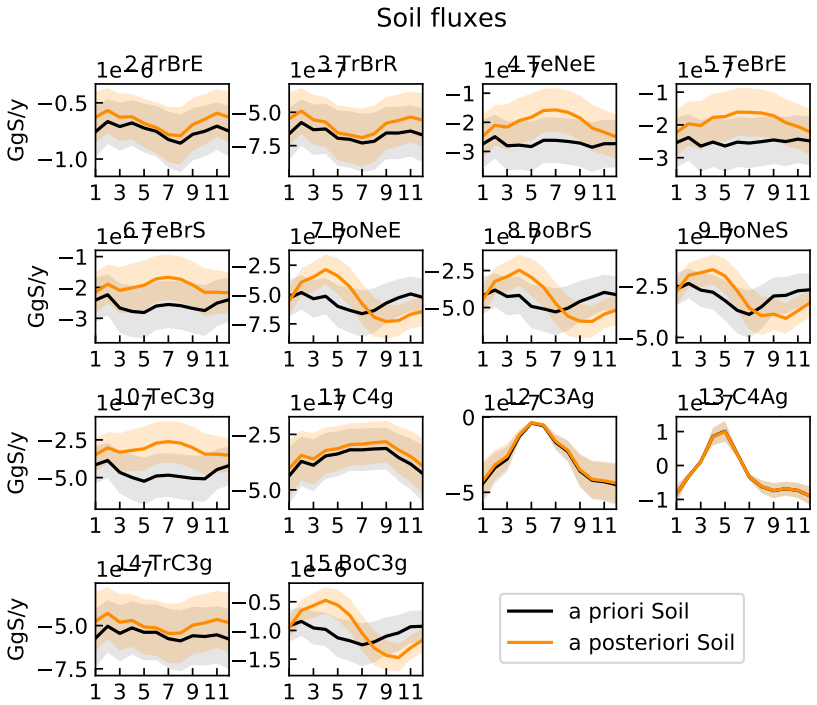

Figure S5. Mean seasonal cycle of the total prior (black) and posterior (orange) soil fluxes and their uncertainties within each of the 15 PFTs. The fluxes have been averaged between 2009-2011. Only the values integrated over the Northern Hemisphere are shown for the PFTs 4, 5, 6, 10, 11, 12, 13.

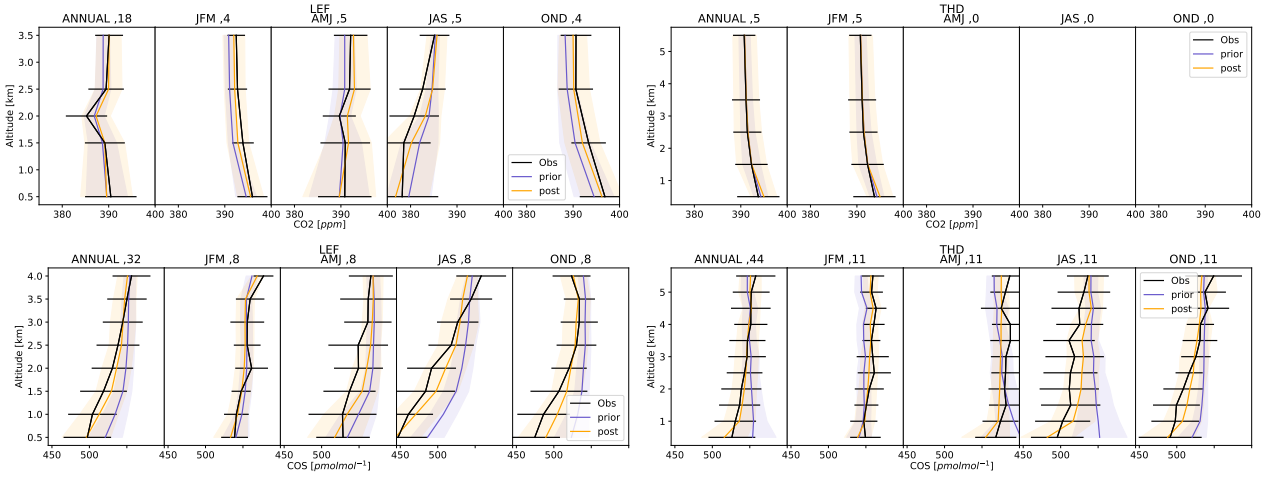

Figure S7. Mean (thick lines) and associated standard deviation (shaded areas) for the monthly CO_2 (top) and COS (Bottom) vertical profile at site LEF (left) and THD (right) during the period 2008–2011. The data have first been averaged in 0.5 km altitude bins per hour and per site. The statistics are drawn from that ensemble of monthly averaged values. They are shown for each season (January–March, JFM; April–June, AMJ; July–September, JAS; October– December, OND) and for the whole year. Because of the unbalanced prior COS and CO_2 budget, the annual mean of the bias at 3.5 km has been removed for the prior vertical profile in order to highlight the differences in profile shape, .

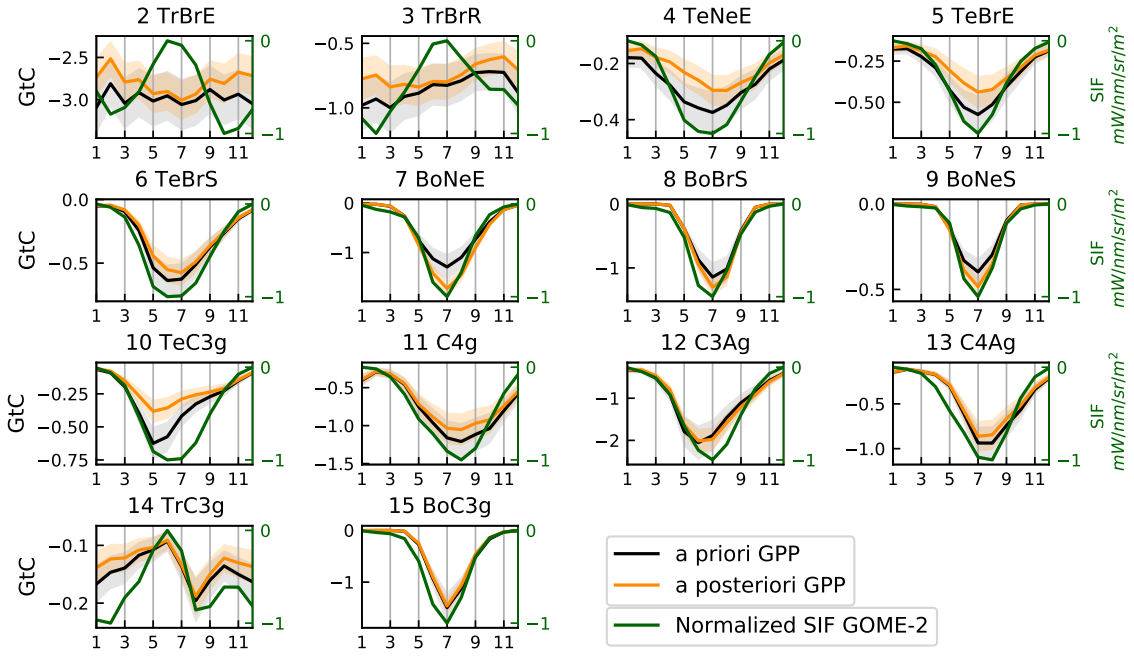

Figure S6. Mean seasonal cycle of the total prior (black) and posterior (orange) GPP fluxes and their uncertainties within each of the 15 PFTs during the period 2009-2018. The mean seasonal cycle of the SIF from GOME-2 has been superimposed on the GPP seasonal cycle in green. The SIF fields have been multiplied by -1 beforehand so that a minimum of SIF corresponds with a minimum of GPP on the picture. The fluxes have been averaged between 2009-2018. PFT 1, the bare soil, is not shown as respiration and GPP are null. Only the values integrated over the Northern Hemisphere are shown for PFTs 4, 5, 6, 10, 11, 12 and 13. The acronyms Tr, Bo and Te mean Tropical, Boreal and Temperate, respectively.

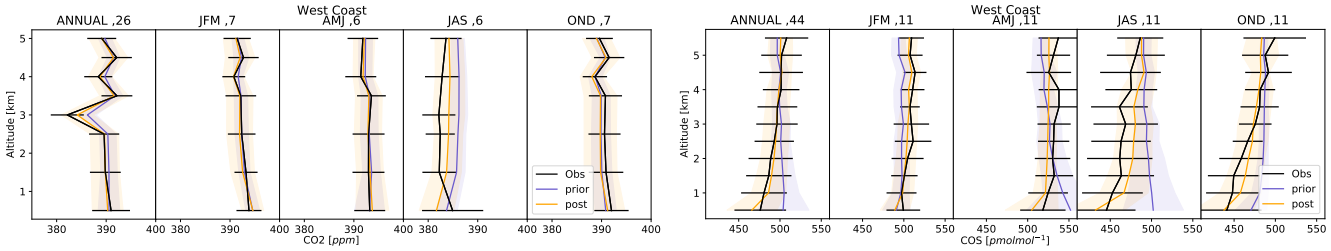

Figure S8. Same Figure as S7 but for the West Coast domain. The West Coast domain is associated with the ESP site.

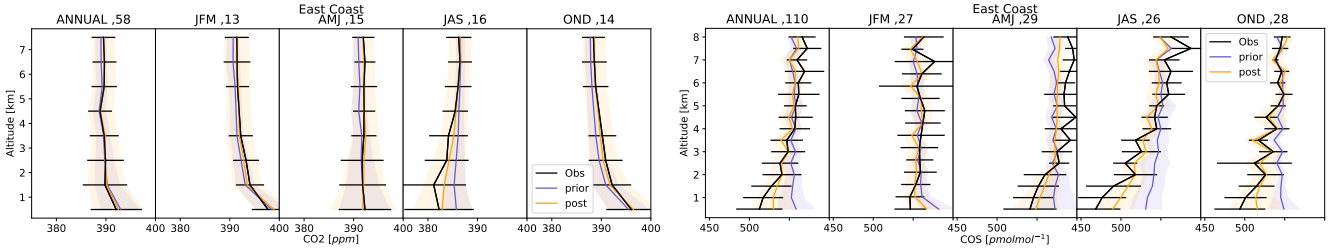

Figure S9. Same Figure as S7 but for the East Coast domain. The East Coast domain encompasses the NHA and CMA.

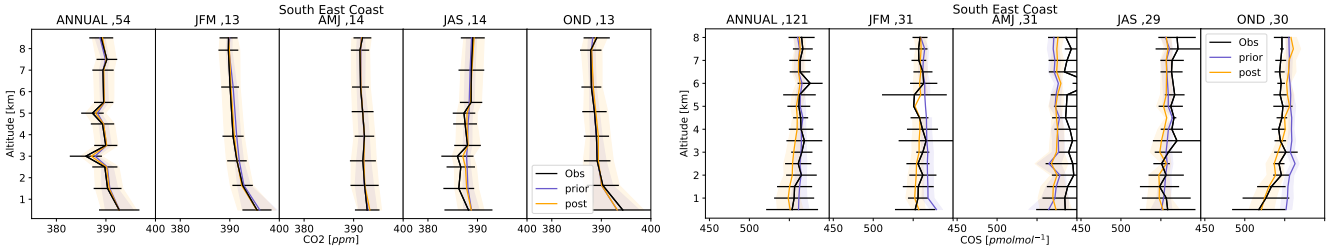

Figure S10. Same Figure as S7 but for the South East Coast domain. The South East Coast domain encompasses the sites SCA and TGC.

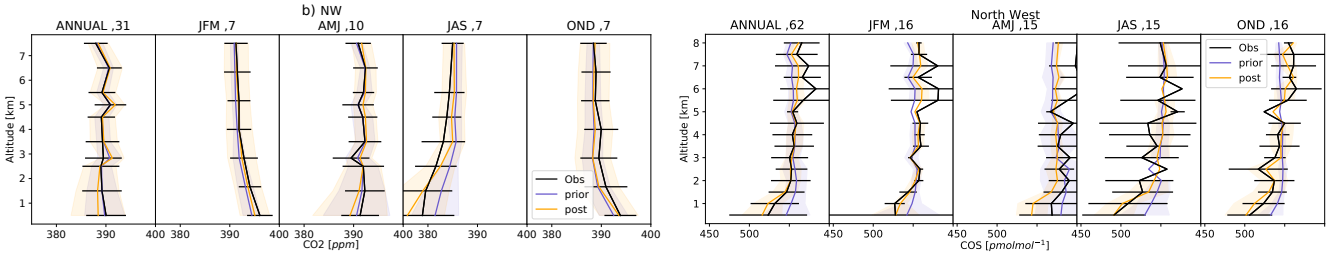

Figure S11. Same Figure as S7 but for the North West domain. The North West domain is associated with the site ETL.

F Supplementary figures of the section 3.3.2 : Evaluation of the simulated concentrations against surface measurements a three japanese sites.

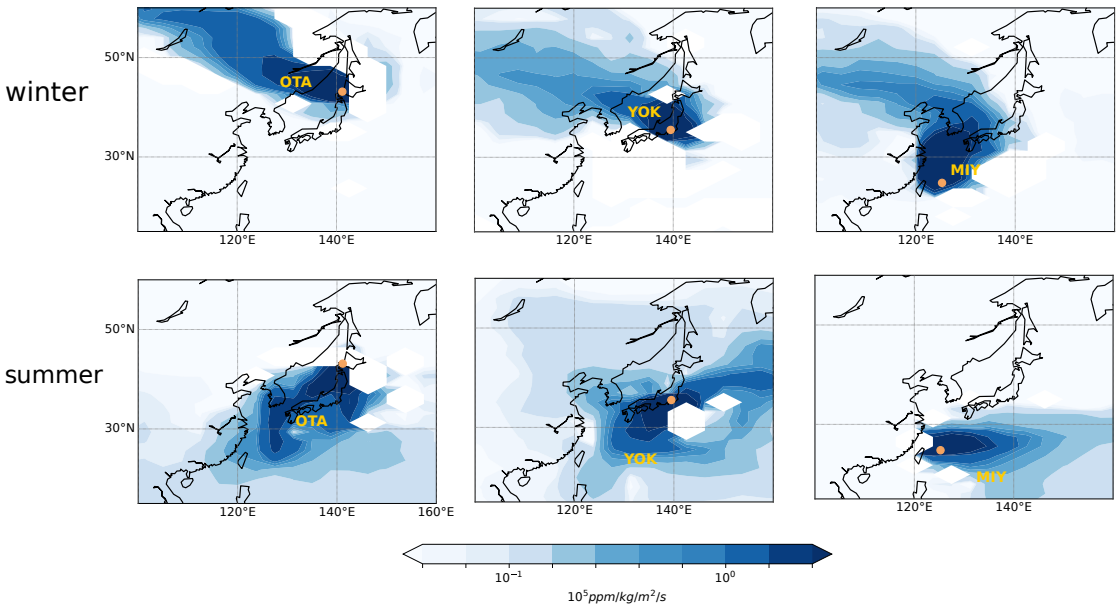

Figure S12. Seasonal climatology (Winter: top and Summer: bottom) of the Jacobians computed by the adjoint of the LMDz model: map of the partial derivatives, in ppm/(kg/m2/h), of a weekly mean concentration for the station OTA (lef), YOK (middle), MIY (right) with respect to CO_2 surface fluxes in the previous month. The yellow dots denote the location of the surface sites. The white areas corresponds to negative sensitivities resulting from the slope limiters introduced in the Van Leer (1977) advection scheme (see Hourdin et al. (2006) for more explanations.)

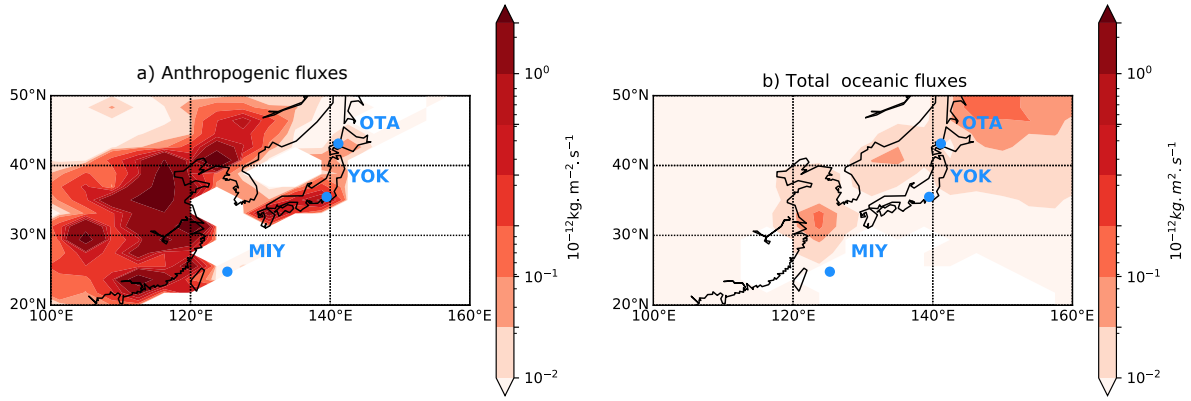

Figure S13. a) Anthropogenic emission map and b) Prior oceanic emission map for summer 2019 (July-August). The blue dots denote the location of the surface sites. The anthropogenic fluxes have been interpolated on the coarser LMDz grid while ensuring mass conservation and therefore don't follow exactly to the python coastlines. The fluxes are the reference fluxes described in section 2.

G Supplementary figures of the section 3.3.2 : Evaluation of the simulated concentrations against surface measurements at GIF

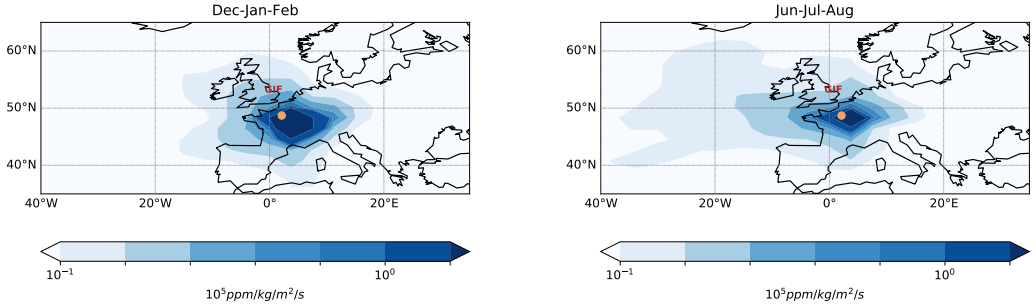

Figure S14. Seasonal climatology (Winter: left and Summer: right) of the Jacobians computed by the adjoint of the LMDz model: map of the partial derivatives, in ppm/(kg/m2/h), of a weekly mean concentration at site GIF with respect to CO_2 surface fluxes in the previous month during the period 2016-2019. The brown dots denote the location of the surface sites.

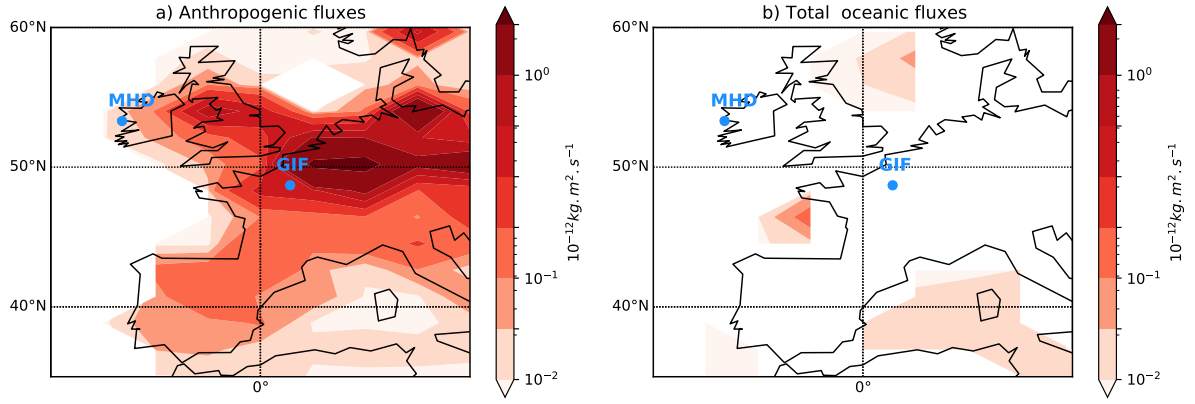

Figure S15. a) Anthropogenic emission map and b) Total oceanic emission map for winter (Dec-Jan-Feb) during the period 2016-2019. The blue dots denote the location of the surface sites. The fluxes have been interpolated on the coarser LMDz grid while ensuring mass conservation. The fluxes are the reference fluxes described in section 2.

H Atmospheric inversion using only CO_2 observations

We performed an atmospheric inversion using only CO_2 observed concentration that we call "INV-CO2". For the purpose of comparison, the standard inversion using CO_2 and COS observations is called "INV-CO2COS".

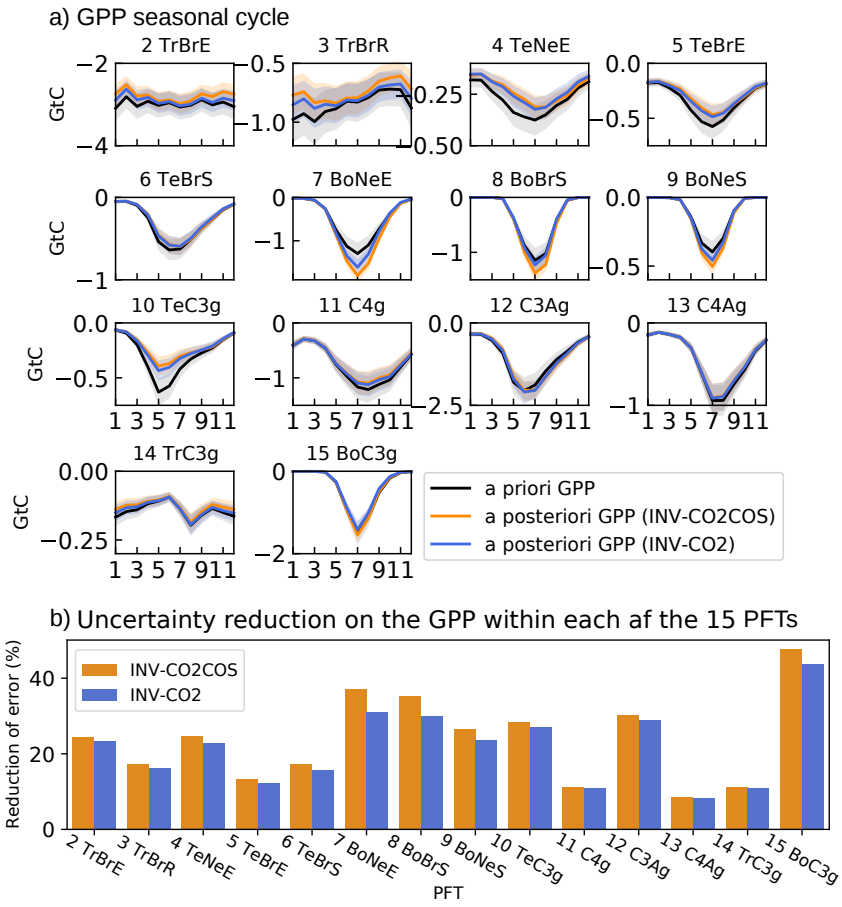

Figure S16. a) Mean seasonal cycle of the total prior (black) and posterior (orange and blue) GPP fluxes and their uncertainties within each of the 15 PFTs during the period 2009-2018. The orange curve is associated with the standart inversion using COS and CO_2 observations. The blue curve is from the inversion using only CO_2 observations. The fluxes have been averaged over 2009-2018. PFT 1, bare soil, is not shown as respiration and GPP are null. Only the values integrated over the Northern Hemisphere are shown for PFTs 4, 5, 6, 10, 11, 12 and 13. The identifiers of the PFTs are described in the manuscript. The acronyms Tr, Bo and Te mean Tropical, Boreal and Temperate, respectively. b) Reduction of error of the GPP within each of the 15 PFTs driven by the inversion using CO2 and COS observations (orange: INV-CO2COS) and CO2 only observations over the years 2009-2019.

I Sampling dates of the COS measurements

J Impact of using an 0 order approach on the vegetation fluxes of COS compared to a order 1 approach

Figure S19 further shows that the order 1 approach has a significant influence on the atmospheric COS concentrations at sites AMA, BRW, HFM. For instance at AMA, the seasonal cycle has decreased of 50 ppt.

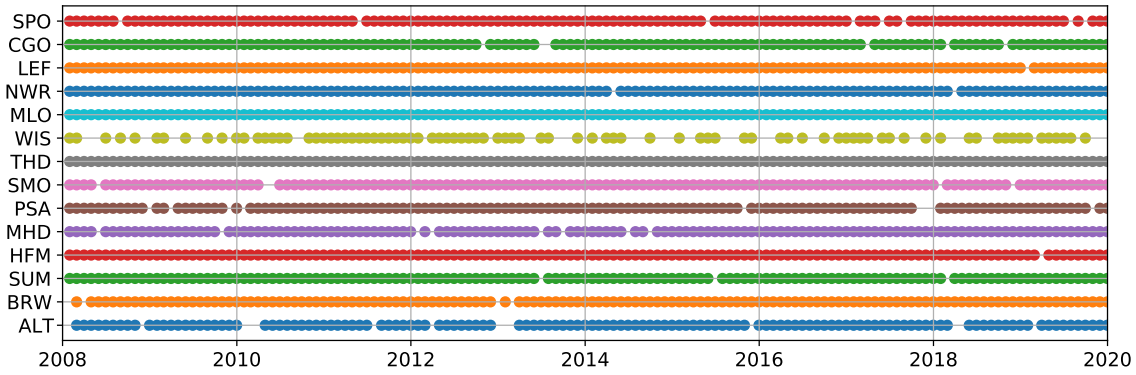

Figure S17. Sampling dates of the COS measurements for the stations of the NOAA network

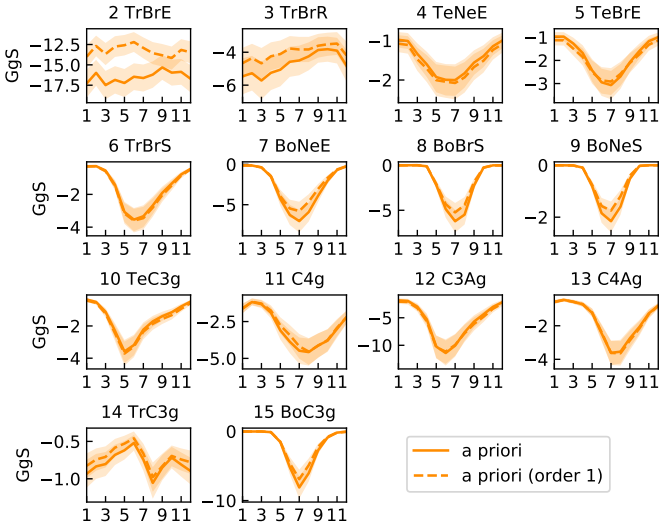

Figure S18. Mean seasonal cycle of the total posterior (orange) and the posterior GPP fluxes with optimized COS concentrations (orange, dashed line) and their uncertainties within each of the 15 PFTs during the period 2009-2018 [FC: la legende sur la figure est incoherente]. The orange curve is associated with the standard inversion using COS and CO_2 observations. The fluxes have been averaged over 2009-2018. PFT 1, bare soil, is not shown as respiration and GPP are null. Only the values integrated over the Northern Hemisphere are shown for PFTs 4, 5, 6, 10, 11, 12 and 13. The identifiers of the PFTs are described in the manuscript. The acronyms Tr, Bo and Te mean Tropical, Boreal and Temperate, respectively.

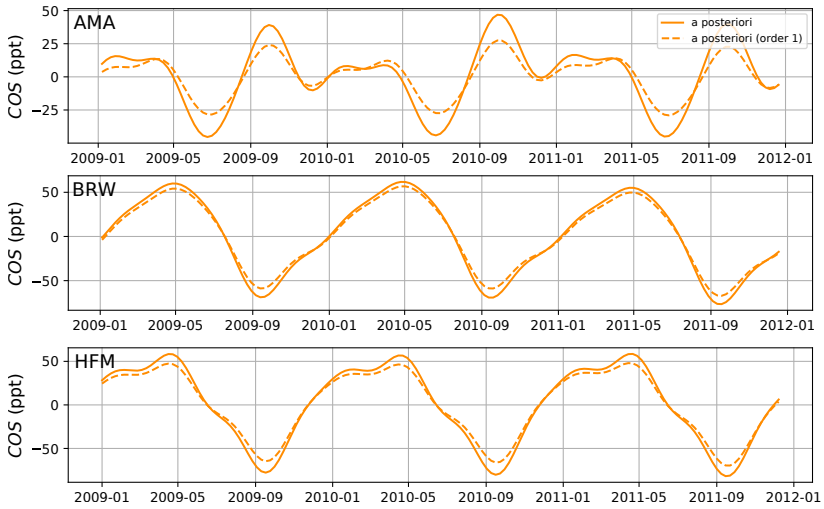

Figure S19. Detrained temporal series of the optimized concentrations using the 0 order approach (full line, orange) and the optimized concentrations using the order 1 approach (dashed line, orange) at sites AMA (top), BRW(middle) and HFM (bottom). The site AMA is located in the Amazon basin in Brazil. The mean differences between the two curves are 40, 30, 50 ppt at BRW, HFM, AMA over the years 2008-2011.

References

Campbell, J. E., Carmichael, G. R., Chai, T., Mena-Carrasco, M., Tang, Y., Blake, D. R., Blake, N. J., Vay, S. A., Collatz, G. J., Baker, I., Berry, J. A., Montzka, S. A., Sweeney, C., Schnoor, J. L., and Stanier, C. O.: Photosynthetic Control of Atmospheric Carbonyl Sulfide During the Growing Season, Science, 322, 1085–1088, https://doi.org/10.1126/science.1164015, https://science.sciencemag.org/content/322/5904/1085, publisher: American Association for the Advancement of Science Section: Report, 2008.

Hourdin, F., Talagrand, O., and Idelkadi, A.: Eulerian backtracking of atmospheric tracers. II: Numerical aspects, Quarterly Journal of the Royal Meteorological Society, 132, 585–603, https://doi.org/10.1256/qj.03.198.B, https://rmets.onlinelibrary.wiley.com/doi/abs/10.1256/qj.03.198.B, _eprint: https://rmets.onlinelibrary.wiley.com/doi/pdf/10.1256/qj.03.198.B, 2006.

Ma, J., Kooijmans, L. M. J., Cho, A., Montzka, S. A., Glatthor, N., Worden, J. R., Kuai, L., Atlas, E. L., and Krol, M. C.: Inverse modelling of carbonyl sulfide: implementation, evaluation and implications for the global budget, Atmospheric Chemistry and Physics Discussions, pp. 1–39, https://doi.org/https://doi.org/10.5194/acp-2020-603, https://acp.copernicus.org/preprints/acp-2020-603/, publisher: Copernicus GmbH, 2020.

Montzka, S. A., Calvert, P., Hall, B. D., Elkins, J. W., Conway, T. J., Tans, P. P., and Sweeney, C.: On the global distribution, seasonality, and budget of atmospheric carbonyl sulfide (COS) and some similarities to CO2, Journal of Geophysical Research: Atmospheres, 112, https://doi.org/10.1029/2006JD007665, https://agupubs.onlinelibrary.wiley.com/doi/abs/10.1029/2006JD007665, _eprint: https://agupubs.onlinelibrary.wiley.com/doi/pdf/10.1029/2006JD007665, 2007.

Van Leer, B.: Towards the ultimate conservative difference scheme. IV. A new approach to numerical convection, Journal of Computational Physics, 23, 276–299, https://doi.org/10.1016/0021-9991(77)90095-X, http://www.sciencedirect.com/science/article/pii/002199917790095X, 1977.